

A synthesis dataset of permafrost thermal state for the Qinghai-Tibet (Xizang) Plateau, China

Lin Zhao^{1,2*}, Defu Zou², Guojie Hu^{2*}, Tonghua Wu², Erji Du², Guangyue Liu², Yao Xiao², Ren Li², Qiangqiang Pang², Yongping Qiao², Xiaodong Wu², Zhe Sun², Zanpin Xing², Yu Sheng³, Yonghua Zhao², Jianzong Shi², Changwei Xie², Lingxiao Wang¹, Chong Wang¹, Guodong Cheng²

¹ School of Geographical Sciences, Nanjing University of Information Science & Technology, Nanjing 210044, China

² Cryosphere Research Station on Qinghai-Xizang Plateau, State Key Laboratory of Cryospheric Sciences, Northwest Institute of Eco-Environment and Resources, Chinese Academy of Sciences, Lanzhou 730000, China

³ State Key Laboratory of Frozen Soil Engineering, Northwest Institute of Eco-Environment and Resources, Chinese Academy of Sciences, Lanzhou 730000, China

Correspondence: Lin Zhao (lzhao@nuist.edu.cn), Guojie Hu (huguojie123@lzb.ac.cn)

Abstract:

Permafrost is important for the climatic, hydrological, and ecological processes on the Qinghai-Tibet Plateau (QTP). The changing permafrost and its impact have been attracting great attention worldwide never before. More observational and modeling approaches are needed to promote an understanding of permafrost thermal state and climatic conditions on the QTP. However, limited data on the permafrost thermal state and climate background were sporadically reported in different pieces of literature due to the difficulties to access to and work in this region, where the weather is severe, environmental conditions are harsh and the topographic and morphological features are complex. From the 1990s, we began to establish the permafrost monitoring network on the QTP. Meteorological variables were measured by automatic meteorological systems. The soil temperature and moisture data were collected from an integrated observation system in the active layer. Deep ground temperature (GT) was observed from boreholes. In this study, a comprehensive dataset after quality control consisting of long-term meteorological, GT, soil moisture and soil temperature data were compiled from an integrated, distributed and multiscale observation network in the permafrost

32 regions of QTP. These datasets were helpful for the scientists with multiple study fields (i.e., climate,
33 cryospheric, ecology and hydrology, meteorology science), which will significantly promote the
34 verification, development and improvement of the hydrological model, land surface process model
35 and climate model on the QTP. The datasets are available from the National Tibetan Plateau/Third
36 Pole Environment Data Center ([https://data.tpsc.ac.cn/en/disallow/789e838e-16ac-4539-bb7e-
37 906217305a1d/](https://data.tpsc.ac.cn/en/disallow/789e838e-16ac-4539-bb7e-906217305a1d/), doi: 10.11888/ Geocry.tpsc.271107).

38

39 **1 Introduction**

40 Permafrost is widely distributed on the QTP, which is called the “Third Pole of the Earth” (Qiu,
41 2008), is about 1.06×10^6 km² in area and accounting for approximately a quarter of the QTP (Zou
42 et al., 2017). Its unique and complicated hydrothermal process has great regulating effects on ground
43 surface moisture, energy and mass exchange, ecosystem stability and carbon cycles (Cheng et al.,
44 2019; Schuur et al., 2011). The surface energy and water cycle over the QTP have great influence
45 on Asian monsoon, East Asian atmospheric circulation and global climate change (Ma et al., 2017;
46 Yao et al., 2017). The characteristics of diabatic heating field of QTP are also used as an important
47 factor for the short-term climate prediction in China (Liu and Hou, 1998; Wu et al., 2009; Ye and
48 Gao, 1979).

49 The permafrost in the QTP has experienced significant degradation in response to climate
50 warming, which mainly manifested as the permafrost area shrinking and ground temperature (GT)
51 rise, the increased active layer, and decreased permafrost thickness (Hu et al., 2019b; Sharkhuu et
52 al., 2007; Wang et al., 2000; Cheng et al., 2019). The permafrost degradation has caused changes in
53 surface vegetation characteristics. It was reported that the area of Alpine meadow on the QTP
54 decreased by 16.2×10^4 km² (accounted for 32.4% of the QTP (Zhao and Sheng, 2015)) in recent
55 decades, which caused the change in hydrological processes and ecological environment and further
56 led to desertification (Cheng and Jin, 2013; Cheng et al., 2019; Wu et al., 2003; Zhao et al., 2019).
57 In addition, permafrost degradation could result in the decomposition of organic matter and
58 greenhouse gases increased, which will finally affect the surface energy balance and the climate
59 system (Wang et al., 2006a; Ping et al., 2015; Schuur et al., 2015; Schuur et al., 2011; Wu et al.,
60 2012; Hu et al., 2019a). Permafrost degradation has also altered the geomorphological features and
61 affected the stability of engineering structures in this region (Zhao et al., 2017).

62 However, the collection of long-term and high-resolution data over the permafrost regions of
63 QTP is challenging due to the complex terrain, severe weather, and inconvenient access (Ma et al.,
64 2008; Li et al., 2012). Previous studies on the permafrost focused on local and site scale and major
65 along the Qinghai-Xizang Highway (QXP)/Railway (Cuo et al., 2015; Su et al., 2013). Some new
66 observation sites in permafrost regions in the vast western territory of the QTP were reported in
67 recent years (Zhao et al., 2017; Zhao et al., 2018; Zhao et al., 2020). Nevertheless, the climate
68 background used in almost all the permafrost studies was based on the only 4 national
69 meteorological stations located within the vast territory of permafrost regions. It is urgent to
70 establish a synthesis observational database of permafrost thermal state and its climatic background
71 to satisfy the requirements of calibration and validation for remote sensing interpretation and
72 hydrothermal processes simulation, and also for the key parameters acquisition in permafrost
73 regions (Bao et al., 2016; Li and Koike, 2003; Wang et al., 2017; Zhang et al., 2008; Hu et al., 2020).
74 The complexity of the dynamic process of water and heat in freeze-thaw cycles is also considered
75 one of the crucial reasons for the great errors in permafrost change simulation (Chen et al., 2014;
76 Hu et al., 2016; Yang et al., 2018). Nevertheless, it is of great significance to provide a set of data
77 in dynamic thermal characteristics of the permafrost on the QTP (Wang et al., 2006b; Zhao et al.,
78 2004).

79 The Cryosphere Research Station on the QTP, Chinese Academy of Sciences (CRS-CAS), has
80 established a comprehensive and widely permafrost monitoring network on the QTP (Zhao et al.,
81 2019, 2020). This network mainly focuses on monitoring permafrost and its environmental factors
82 in high-elevation and cold-climate regions of the QTP. Since the station was established in 1987,
83 we have conducted long-term continuous monitoring and large-scale field investigations on
84 permafrost. Thus, it synthetically studied the mechanisms of the change in hydrothermal conditions
85 permafrost and their simulations and ecological effects. This paper firstly integrated air temperature,
86 GT, soil moisture and permafrost temperature dataset over the permafrost regions across QTP from
87 the CRS-CAS monitoring networks. The monitoring network is summarized in Sect. 2. In Sect. 3,
88 the datasets are described in detail. In Sect. 4, the data availability and access are provided, and in
89 Sect. 5, the conclusions and future work are summarized.

90 **2 Monitoring networks and data processing**

2.1 Permafrost monitoring networks

The vegetation in the permafrost region of the QTP is mainly alpine meadow, swamp meadow, alpine steppe, and alpine desert (Wang et al., 2016). The soils in the western permafrost region are Gelisols, Inceptisols and Aridisols, and in the eastern mainly consists of Gelisols, Mollisols and Inceptisols (Li et al., 2015). The permafrost monitoring network includes 6 automatic meteorological stations (AMSs), 12 active layer sites and, 84 boreholes (Fig. 1, Table 1), which were primarily selected based on the landforms and underly surface conditions (e.g., the vegetation and soil characteristics) along the Qinghai-Xizang Engineering Corridor and in each investigated region of the QTP. The elevation of all the sites is higher than 4000 m a.s.l (31.82~37.75 °N, 77.58~99.50 °E).

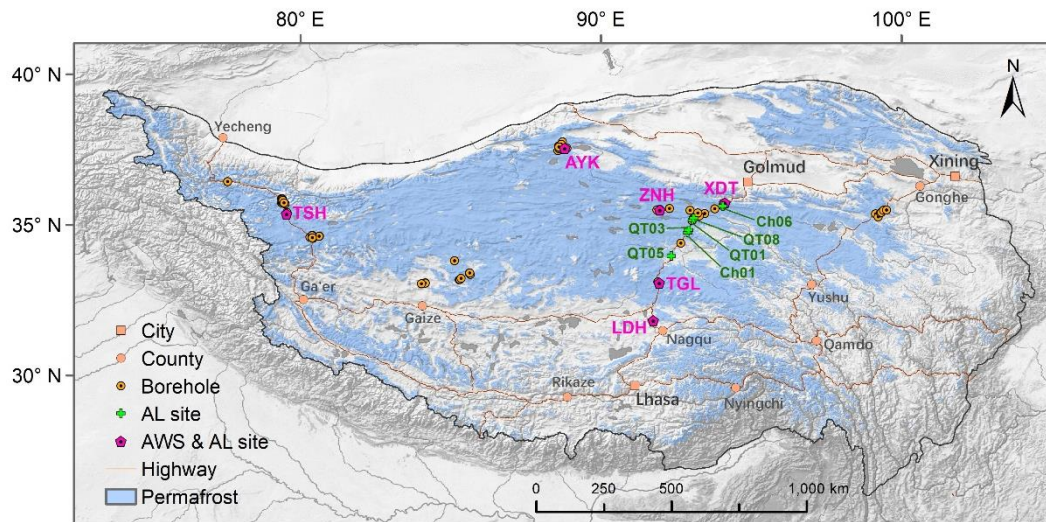
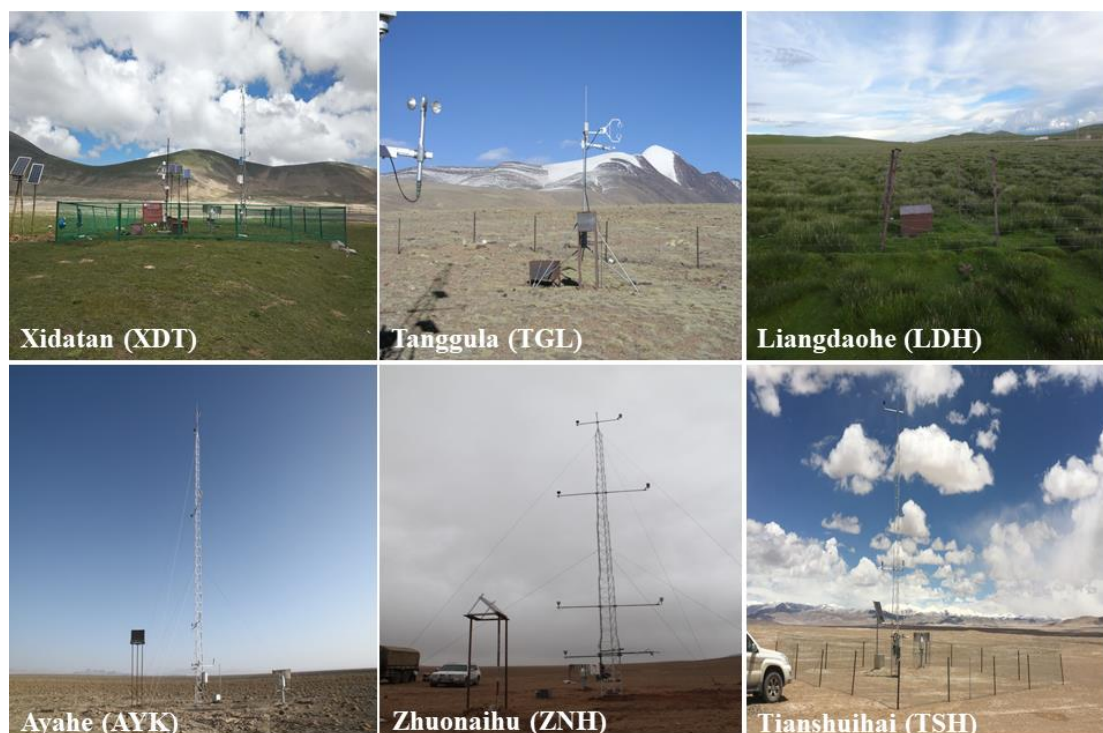


Figure 1. The permafrost monitoring networks on the QTP. AL: active layer; AWS: automatic meteorological station

We set 6 AMSs (Fig. 2) within the permafrost zone since 2004. The main observation indices include air temperature, humidity, wind speed gradient observation, radiation balance, and precipitation, etc. The active layer observation system and GT borehole were set up simultaneously to record the permafrost, climate, vegetation, soil indices in different regions of the QTP. Liangdaohe (LDH) site has the lowest latitude, and it gets the warmest air temperature and the largest annual precipitation, while Tianshuihai (TSH) and Ayake (AYK), located in the northwest and north of the QTP, respectively, have the minimum and penultimate temperatures and annual precipitations. TSH has the highest solar radiation among the 6 stations.

Xidata (XDT) and Tanggula (TGL) are two sites with the most extended sequence of 6 gradient

113 meteorological stations. They were established in May 2004 and data sequences are over 16 years.
 114 XDT is located near the northern permafrost boundary of the QTP, and represents the characteristics
 115 of the island permafrost. TGL site is located on the north side of the Tanggula Mountains in the
 116 hinterland of the QTP and represents the characteristics of the continuous permafrost area. LDH is
 117 located near the southern boundary of the permafrost region and represents the characteristics of the
 118 discontinuous permafrost region. ZNH is located in the Hoh Xil region, where there was no
 119 meteorological station and even no in situ meteorological monitoring data ever before. It fills the
 120 data gap in the central and northern areas of the QTP and is also located in a continuous permafrost
 121 area. AYK is located in the Altun Mountains area in the northern Tibetan Plateau, a vast unmanned
 122 area on the QTP, and is one of the areas with few observations. TSH is located in the West Kunlun
 123 Mountain area near the western border of the permafrost region on the QTP. It can reflect the
 124 regional characteristics of arid, cold, and high altitude in the vast western part of the QTP. The GT
 125 and soil moisture observed of the active layer and permafrost were summarized in Table 1.



126
 127 **Figure 2.** The six comprehensive meteorological stations

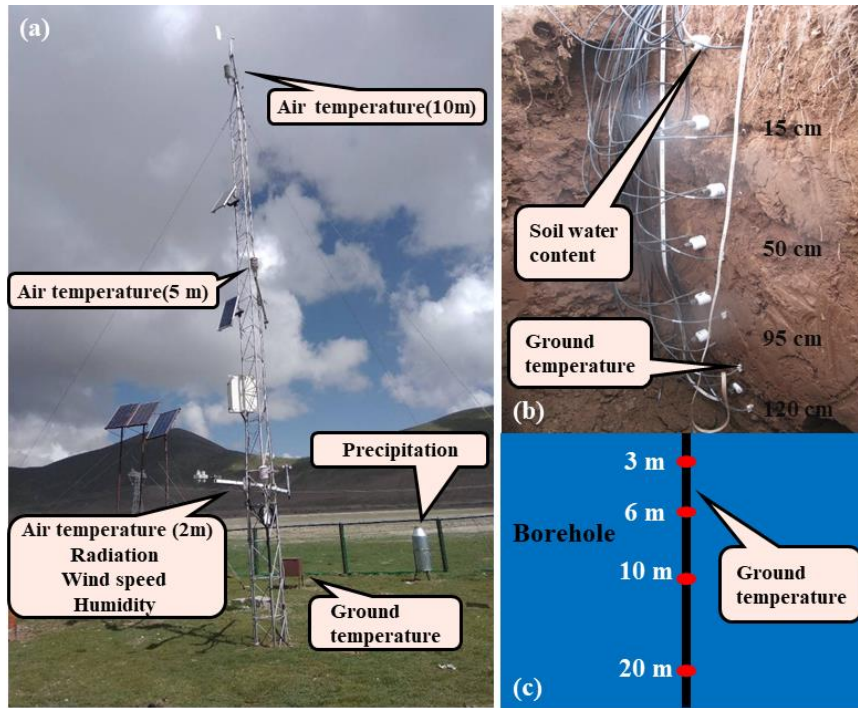
128 **Table 1** The observation instruments and items for meteorological data, ground temperature and soil water content

Observation site type	Available sites	Observation item	Instrument	Accuracy	Height/Depth	Frequencies
Meteorological Stations	6	Upward/downward short-wave radiation	CM3, Kipp & Zonen, Holland	±10%	2 m	1/2 hour

		Upward/downward long-wave radiation	CM3, Kipp & Zonen, Holland	±10%	2 m	
		Air temperature	HMP45C, Vaisala Finland	±0.5 °C	2, 5, 10 m	
		Air humidity	05103_L/RM, Campbell, USA	±3% RH	2, 5, 10 m	
		Wind velocity	T-200B Precipitation Gauge	±0.3 m/s	2, 5, 10 m	
		Precipitation		±0.1 mm	5 m away	
Active Layer	12	Soil temperature	105T/109 Thermocouple temperature sensor	±0.1 °C ±0.2 °C	0.5 m, 1.0 m, 2 m, >2 m	1/2 hour
		Soil moisture content	CS616/ Hydra Soil moisture sensor	±2.5%		
Borehole (automatic)	15	Ground Temperature	Thermistor, SKLFSE, CHINA	±0.05 °C	3, 6, 10, 20 m	1 hour
Borehole (manual)	69	Ground Temperature	Thermistor, SKLFSE, CHINA	±0.1 °C	10, 20 m	1 year

129 2.2 Monitoring data

130 The main observation items and instruments for the meteorological observations were shown
131 in Table 1. The observation was done every 10 minutes and was averaged and recorded every 30
132 minutes automatically. The data were recorded by CR10X, CR1000 and CR3000 data logger
133 (Campbell Scientific). Meteorological data (e.g., the precipitation, radiation, air temperature,
134 relative humidity and wind speed) were recorded hourly with a CR1000/CR3000 data acquisition
135 instrument (Campbell Scientific Inc., USA) (Fig 3a). There were three measured at heights of 2 m,
136 5 m and 10 m for air temperature, relative humidity and wind speed (Table 1).



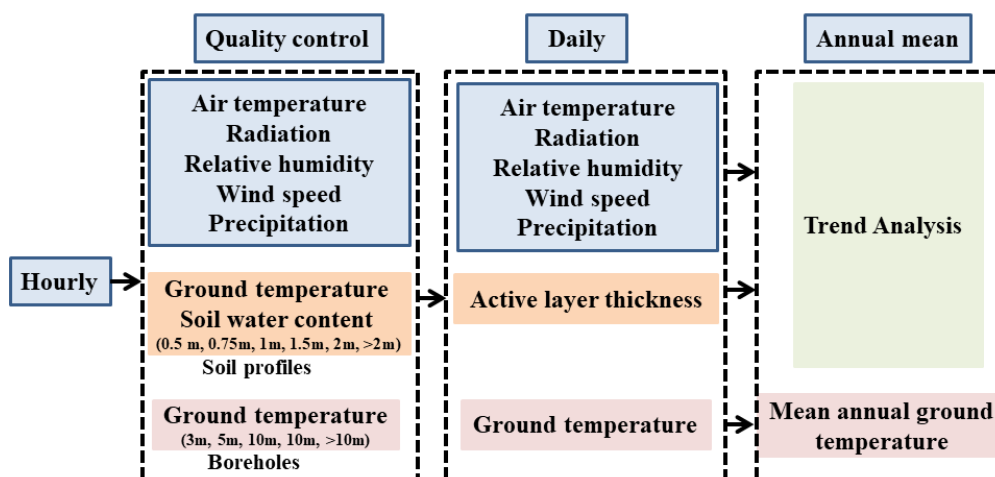
137
 138 **Figure 3.** The comprehensive observation system: (a) meteorological observation, (b) ground temperature and soil
 139 water content in the active layer and (c) ground temperature observation for permafrost.

140 The GT for the active layer monitoring system was measured at different depths from ground
 141 surface to the depth of 10 to 50 cm below the permafrost table with a 105T/109 thermocouple Probe
 142 with an accuracy of $\pm 0.1\text{ }^{\circ}\text{C}/\pm 0.2\text{ }^{\circ}\text{C}$ in the active layer (Fig 3b). The soil water content was
 143 measured by a Hydra soil moisture sensor (Table 1) by connecting to a CR10X/CR1000/CR3000
 144 data logger (Campbell Company, USA).

145 The GT in the borehole was measured by the Thermistor (with an accuracy of $\pm 0.1\text{ }^{\circ}\text{C}$)
 146 produced by the State Key Laboratory of Frozen Soil Engineering, Cold and Arid Regions
 147 Environmental and Engineering Research Institute of the Chinese Academy of Sciences (SKLFSE,
 148 CAREERI, CAS), which were downloaded to the depths of 3 m, 6 m, 10 m and 20 m depths within
 149 a steel pipe in the boreholes. All the borehole GTs along the QXH and located at the same sites with
 150 AMSs were measured at 15 minutes. The averaged value for each hour was automatically recorded
 151 by data loggers (CR1000/ CR3000, Campbell Scientific Company, Logan, UT, USA). Moreover,
 152 all the other boreholes far away from the QXH were measured manually by a digital multimeter
 153 once for one or two years according to the local transportation, financial supports, etc. (Table 1)
 154 (Fig 3c).

155 **2.3 Data processing workflow**

156 The data processing workflow is showed in Fig. 4. The quality control was two-fold: (1) the
 157 missing data were replaced by -6999; (2) the singular unphysical data were rejected, and the gaps
 158 were replaced by -6999. In addition, all the daily data were calculated by every 30 min (1 h) interval
 159 per day for the data collected by data loggers. The instruments at meteorological stations are
 160 calibrated every few years by comparing observations with standard instruments for about one week.
 161 The active layer thickness was derived by the maximum depth of 0 °C isotherms from linear
 162 interpolation of the daily maximum GT. The monthly and annual mean air and GTs, radiation, wind
 163 speed, relative humidity and soil water content were also analyzed. The trend of air temperature,
 164 active layer thickness, and GT is analyzed and provided at the stations with long-time observation.
 165 GTs from manually monitoring boreholes were quality controlled for every measurement.



166

167 **Figure 4.** Schematic diagram of data processing workflow used to compile the permafrost dataset on the QTP.

168 3 Data description and evaluation

169 3.1 Meteorological data

Table 2. The information of six meteorological stations

Sites	XDT	TGL	LDH	ZNH	AYK	TSH
Elevation (m a.s.l)	4538	5100	4808	4784	4300	4844
Ta (°C)	-3.6	-4.7	-2.3	-4.9	-5.2	-6.0
RH (%)	53.5	51.5	48.2	53.9	46.1	40.6
Precipitation (mm)	384.5	352.0	388.6	277.8	158.6	103.3
Wind speed (m/s)	4.1	4.1	3.2	4.7	4.5	

DSR (W/m ²)	224.2	233.4	231.4	204.8	198.2	250.8
USR (W/m ²)	66.8	61.4	46.6	46.3	53.8	68.5
DLR (W/m ²)	223.0	214.8	237.2	233.8	223.0	211.5
ULR (W/m ²)	304.5	304.5	315.9	303.2	307.6	311.3
Net radiation	75.9	82.3	106.0	89.2	59.8	82.5

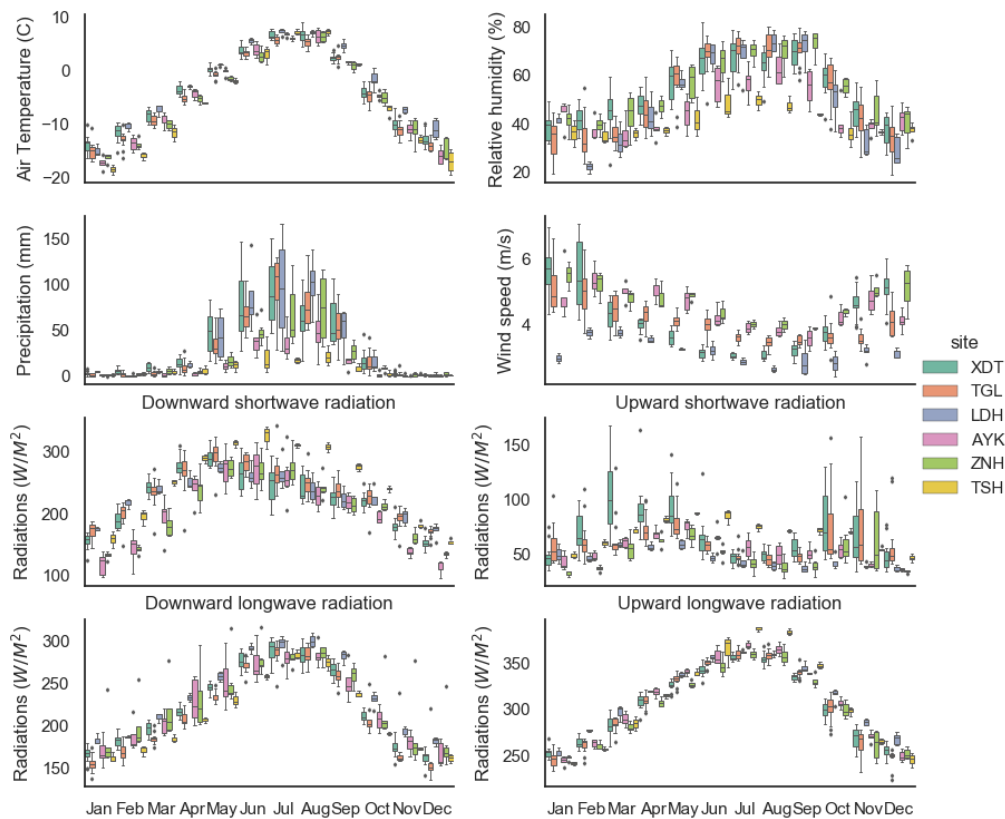
170 The seasonal (spring (Mar.–May), summer (Jun.–Aug.), autumn (Sept.–Nov.), and winter
171 (Dec.–Feb.)) variation of air temperature at all 6 sites is significant with the annual mean from -2.3
172 to -6 °C (Fig. 5). The mean monthly air temperatures in summer are positive but are lower than 0
173 °C in the other 3 seasons. The differences in the air temperatures between 6 stations were minimal
174 in summer, evident in spring and autumn, and much prominent in winter, mainly caused by the
175 difference in altitude and latitude.

176 Significant seasonal variation of precipitation is closely related to the monsoon cycles. From
177 May to September, precipitation accounts for more than 85% of its annual amounts at the 5 sites
178 other than TSH (78.6%). Most of the precipitation is concentrated in summer. A small amount is in
179 late spring and early autumn and rare in the winter. Precipitation has a significant spatial difference,
180 which is more than 350 mm on average at XDT, TGL, LDH along QXH. The precipitation at ZNH,
181 located in the hinterland of the QTP and about 200 km from the QXH, is slightly lower, while it is
182 about 150 mm (slightly higher than half at ZNH) in AYK, which is located on the northern edge of
183 the QTP and has the highest latitude among all the 6 sites. The annual total precipitation at TSH,
184 located near the western boundary of QTP, is the lowest of all the observation sites and is only 100
185 mm.

186 The seasonal variation of air humidity is very consistent with the seasonal variations in air
187 temperature and precipitation. The difference between the stations is related to the precipitation,
188 especially in summer. Due to the scarce precipitation, the relative humidity at TSH and AYK is low
189 throughout the year. It is worth noting that the relative humidity in TGL and LDH is quite low in
190 winter due to these 2 sites are located in relatively lower latitude compared with the other 4 stations.
191 The air temperatures in winter at these 2 stations are relatively higher. The wind speeds at all stations
192 are generally high except LDH. The average annual wind speeds are higher than 4 m/s. The wind
193 speed is the highest in winter, followed by spring and the lowest in summer. The wind speed of

194 LDH was the lowest throughout the year in all AMSs, primarily due to its geomorphological
 195 location, as it is a well-developed basin covered with swamp meadow.

196 Downward short-wave radiation (total solar radiation) usually reaches its maximum in May
 197 and decreases in summer due to rainy- and cloudy-day influences at most sites except TSH. The
 198 mean downward short-wave radiation in summer is only slightly higher than that in spring. However,
 199 at TSH (with little precipitation), it is very high in summer and significantly higher than other sites
 200 in spring and autumn. The upward short-wave radiation is mainly restricted by the surface albedo.
 201 Its high value mainly appeared in autumn and indicated that snow falling events mainly occurred in
 202 autumn, followed by spring and relatively little in winter. The upward short-wave radiation of TSH
 203 in all seasons is high, related to dry and “snow-like” salt-rich ground surface caused by low
 204 precipitation but very high evaporation. The upward and downward long-wave radiation is closely
 205 related to air temperature and surface temperature, respectively, and their seasonal variation trend
 206 is basically consistent with the change of air temperature.

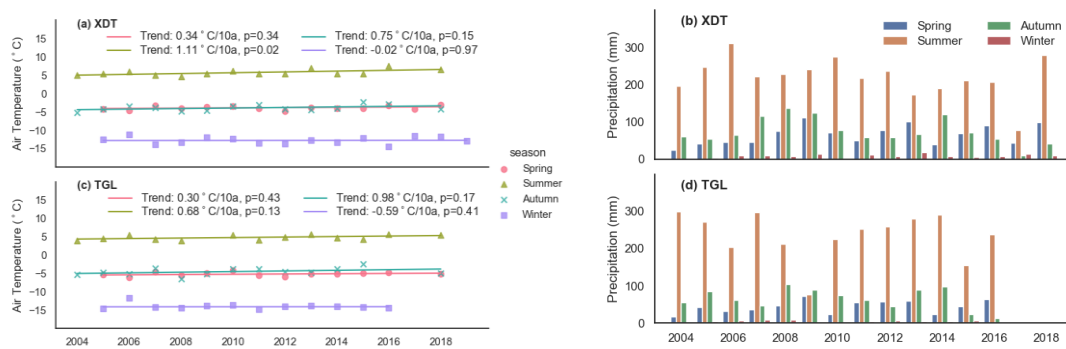


207

208 **Figure 5.** Characteristics of monthly observation variables at six meteorological stations

209 XDT and TGL stations had the data series with a longer period (from 2004 then) and can

210 provide basic data for physical process research and land surface process model research. The
 211 annual mean temperature of the two stations showed increasing trends, with rates of 0.66 and 0.40
 212 °C/10a, and p-values of 0.27 and 0.23, respectively. The warming trend is the highest in summer
 213 and autumn. However, the air temperature in winter shows a slight decrease. The precipitations
 214 show an insignificant week decrease trend (-15.0 and -14.3 mm/10a). It shows a slightly decreasing
 215 trend in summer and autumn and an increasing trend in spring (Fig. 6). The changing trend in air
 216 temperature and precipitation from these 2 stations was almost entirely contrary to the results from
 217 previous researches, which might be due to the limited monitoring time series.



219 **Figure 6.** Seasonal mean series and changes of temperature and precipitation at XDT and TGL
 220 from 2004 to 2018

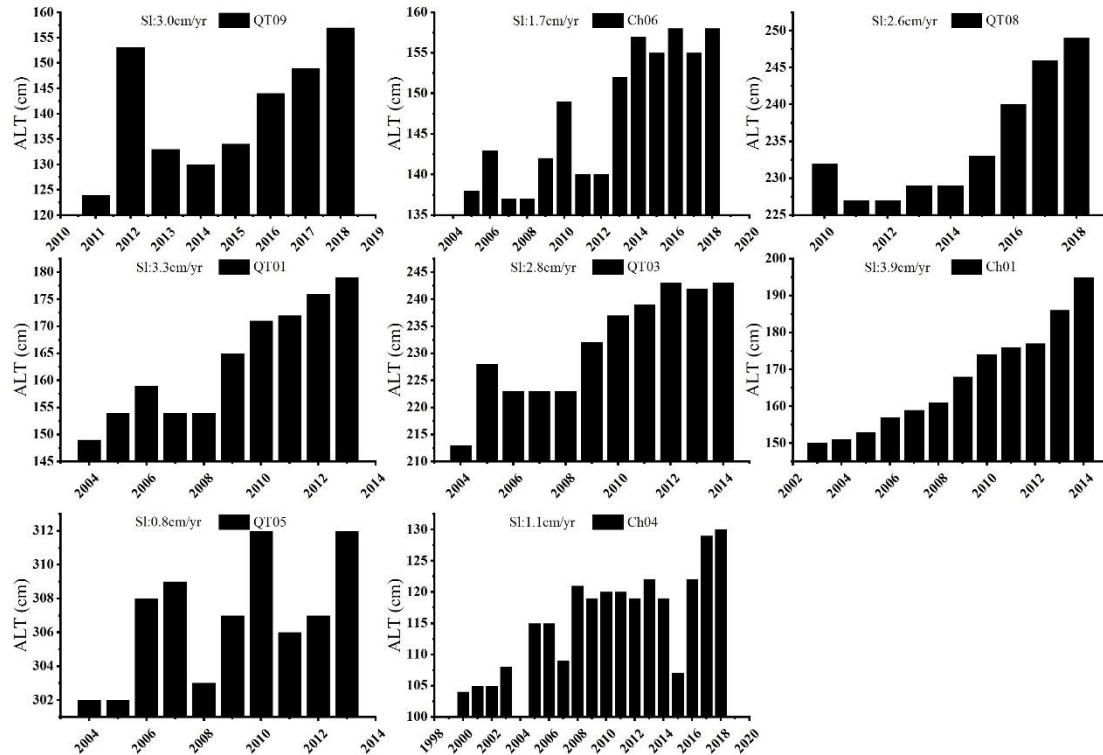
221 3.2 Active layer data

222 3.2.1 Variation of active layer thickness

223 The active layer thicknesses varied from about 120 cm to about 300 cm along Qinghai-Tibet
 224 highway under different surface vegetation conditions (Fig.7). Ch04, which locates at sporadic
 225 island permafrost of the QTB southern permafrost distribution limit regions under swamp meadow
 226 condition, appeared as the shallowest active layer site. Its average thickness was 116cm during the
 227 years 2000-2018. The deepest active layer appeared at QT05, which locates at the margin of
 228 permafrost from taliks formed by the thermal influences from the tributaries of Yangtze River
 229 headwaters, Tongtian river and Tuotuo river. Its average thickness was 307cm from 2004 to 2013,
 230 where the surface vegetation is alpine meadow. In the continuous permafrost zone of QTP, including
 231 Ch06, QT08, QT01, QT03, and Ch01 sites, the shallowest active layer is located at the Kunlun
 232 Mountains pass (Ch06) under nearly bare land surface vegetation condition with an average

233 thickness of 147 cm during 2005-2018. The deepest active layer is located at Wudaoliang (QT08)
234 under bare land with an average thickness of 235 cm during 2010-2018. For representative alpine
235 meadow conditions (e.g., QT01 at Wudaoliang and Ch01 at Fenghuo Mountains), their average
236 thicknesses were 163 cm and 167 cm. While at Beiluhe (QT03), about 10 km north of Ch01 site, its
237 average thickness was about 231 cm with typical alpine meadow condition, which is larger than
238 QT01 and Ch01. In addition, the QT09 called Xidatan is located at the north boundary of the
239 permafrost region with an average active layer thickness of 141cm during 2011-2018 under typical
240 alpine meadow conditions. Overall, in our opinion, the ground surface vegetation conditions may
241 have some influences on active layer thickness spatial distribution. However, it is not a controlling
242 factor, especially at a large spatial scale. The spatial distribution of active layer thickness was jointly
243 influenced by climate conditions, GT (including ground surface temperature and permafrost layer
244 temperature), soil water content, soil texture. Due to the great spatial variation of these above
245 influencing factors, the active layer thickness within our monitoring regions presented as a great
246 spatial variation.

247 In terms of time variation, all the monitoring sites showed the same pattern. Their active layer
248 thicknesses were increasing gradually. Their increasing rate was very different from sites, with the
249 largest increasing rate of 3.9 cm/yr at Ch01 and the lowest increasing rate of 0.8 cm/yr at QT05. Of
250 which worth noting is that the active layer thickness increasing rate is susceptible to the statistical
251 period. For instance, the average increasing rate of QT09 was 3.0 cm/yr during 2011-2018. While
252 during 2014-2018, its average increasing rate was 6.9 cm/yr. Thus, the increasing statistical active
253 layer thickness rates cannot be considered a long-term thickness increasing trend. It only revealed
254 that the active layer thickness has a slow increase trend with inter-annual fluctuation, and their
255 increasing amplitudes are very different amount different monitoring sites.



256

257 **Figure 7.** Variation in active layer thickness among different sites. SI represents the active layer thickness average
 258 annual increasing rate.

259 3.2.2 Temperature in the active layer

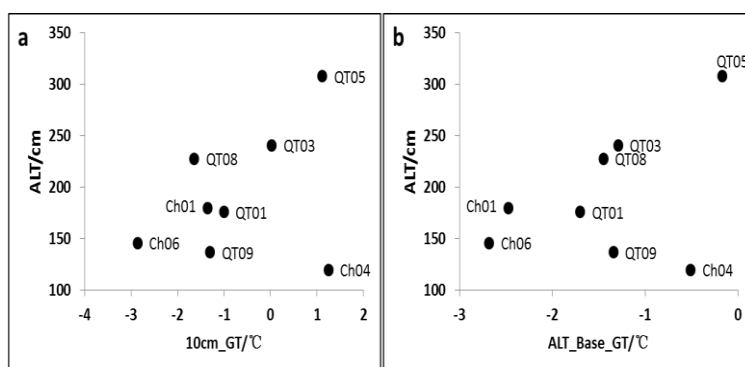
260 In this section, we choose GT at 10cm depth and the base of the active layer from 2011 to 2013,
 261 during which continuous GT monitoring data series of all eight active layer monitoring sites were
 262 available, to analyze the active layer GT spatial distribution and their influence on active layer
 263 thickness spatial distribution (Table.3). The GT (ALT_Base_GT) was derived from geothermal
 264 interpolation when there was no temperature probe at the actual active layer depth position at the
 265 base of the active layer. For all 8 active layer monitoring sites, the mean annual GT (10 cm_GT)
 266 varied greatly from site to site at 10cm depth. The lowest 10 cm_GT appeared at Kunlun Mountains
 267 region (Ch06), which is -2.86 °C. For QT03, QT05 and Ch04, the 10cm_GT were positive and as
 268 high as 1.12 °C and 1.25 °C at sites QT05 and Ch04. For ALT_Base_GT, the relatively low
 269 temperature all appeared at mountain regions, such as Ch06 at the Kunlun Mountains and Ch01 at
 270 Fenghuo Mountains. This because the ALT_Base_GT was simultaneously influenced by ground
 271 surface temperature and underlain permafrost temperature, and in mountains regions, the permafrost
 272 layer temperature is often very low in QTP. At the marginal regions of permafrost distribution or

273 island permafrost, such as QT09, QT05 and Ch04, the ALT_Base_GT were relatively higher than
 274 other sites due to their high underlain permafrost layer temperature.

275 **Table. 3** The mean active layer thickness, ground temperature at depth of 10 cm and permafrost table

Sites Name	ALT/cm	10cm_GT/°C	ALT_Base_GT/°C
QT09	137	-1.3	-1.34
Ch06	146	-2.86	-2.68
QT08	228	-1.64	-1.45
QT01	176	-1	-1.7
QT03	241	0.03	-1.29
Ch01	180	-1.35	-2.47
QT05	308	1.12	-0.17
Ch04	120	1.25	-0.51

276 The scatter plot between active layer thickness and 10cm_GT showed that, on the whole, ALT
 277 increased with the increase of 10cm_GT, but they are not linear dependent (Fig.8a). Especially for
 278 Ch04 at island permafrost region under swamp meadow surface vegetation, the relationship between
 279 ALT and 10cm_GT was very different from other monitoring sites, demonstrating that surface GT
 280 spatial distribution did influence ALT distribution. However, it cannot be used as a primary control
 281 factor for ALT prediction under different soil and vegetation conditions. In contrast to the
 282 relationship between ALT and 10 cm_GT, the relationship between ALT and ALT_Base_GT is
 283 much better (Fig. 8b). If without considering the large deviation of sites QT09 and Ch04, active layer
 284 thickness was nearly linear dependent on the variation of ALT_Base_GT, which indirectly showed
 285 that the underlain permafrost temperature properties have a great influence on ALT distribution.



286
 287 **Figure 8.** The relationship between active layer thickness and the temperature of the permafrost table

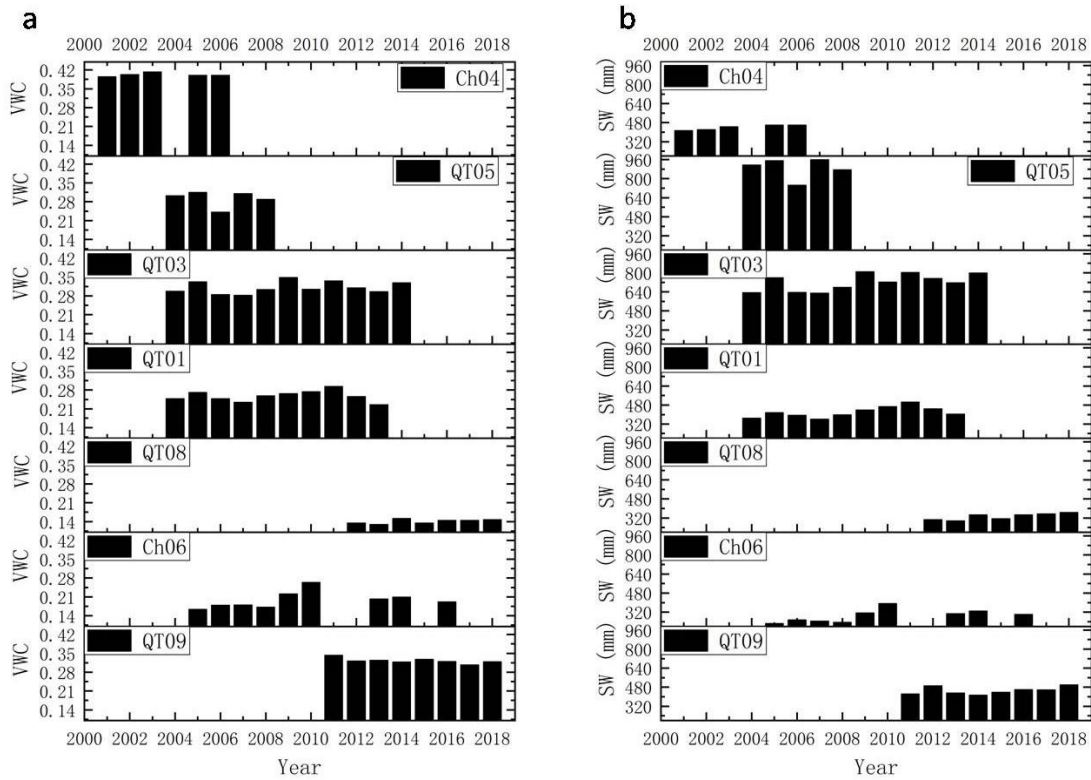
288 The shallow GT of 8 active-layer monitoring sites was collected with automatic data loggers
289 along the Qinghai-Tibetan Road in the dataset. The 10-cm annual mean GT was ranged from -2.62 °C
290 to -0.20 °C for all sites, while ranged from -2.69 °C to -0.37 °C near the top of the permafrost. The
291 temperature at two depths has a good linear correlation. The mean GTs near the top of permafrost
292 at 6 sites were 0.30 °C to 1.83 °C lower than that of 10 cm. At only 2 sites (CN06 and QT08), the
293 former is slightly higher than the latter (approximately 0.2 °C). The subsurface GT of 10 cm at all
294 the sites showed increasing trends with increased rates ranging from 0.03 °C to 0.19 °C per year.
295 The maximum rate occurred at site QT09 which locates the northern marginal region of permafrost.
296 The increasing rate at the bottom of the active layer (near top of permafrost) is slightly lower than
297 the rate of surface active layer. Even at CN06, there was a slight cooling trend at the bottom of the
298 active layer.

299 **3.2.3 Soil moisture in the active layer**

300 The average volumetric soil water content (VWC) within ALT was calculated with a depth-
301 weighted average method when the ground surface began to freeze and ALT reached its max
302 thawing depth at each monitoring site (Fig.9a). In terms of inter-annual change, VWC had no
303 obvious changing trend with random inter-annual fluctuations. In terms of spatial variation, the
304 VWC varied from 0.141 to 0.403 m³/m³ among our monitoring sites, with the largest VWC at Ch04
305 and the lowest at QT08. Active layer soil water content was basically controlled by ground surface
306 vegetation conditions, soil texture and local drainage conditions. For example, a swamp meadow at
307 Ch04 with about 60 cm depth of peat soil layer beneath the ground surface resulted in the very
308 shallow active layer thickness and nearly saturated soil water content condition. At QT05, the soil
309 pit excavated in 2007 revealed that it was sand within 140cm. This site has terrible drainage
310 conditions and resulted in relatively high VWC, averaged 0.292 m³/m³ during 2004-2018. While at
311 QT08, where the soil type is also sand within the active layer, because of its excellent drainage
312 conditions, VWC is very low, averaged 0.141 during 2012-2018.

313 Converting the VWC into total soil water depth per unit area stored within the active layer, soil
314 water depth varied from 290 mm to 890 mm among our monitoring sites (Fig.9b). QT05 had the
315 highest soil water depth, averaged 890 mm during 2004-2008. High soil water depth must absorb
316 high heat energy during the active layer thawing process, explaining why the active layer thickness

317 increasing rate was very low, while its ground surface temperature was very high.



318

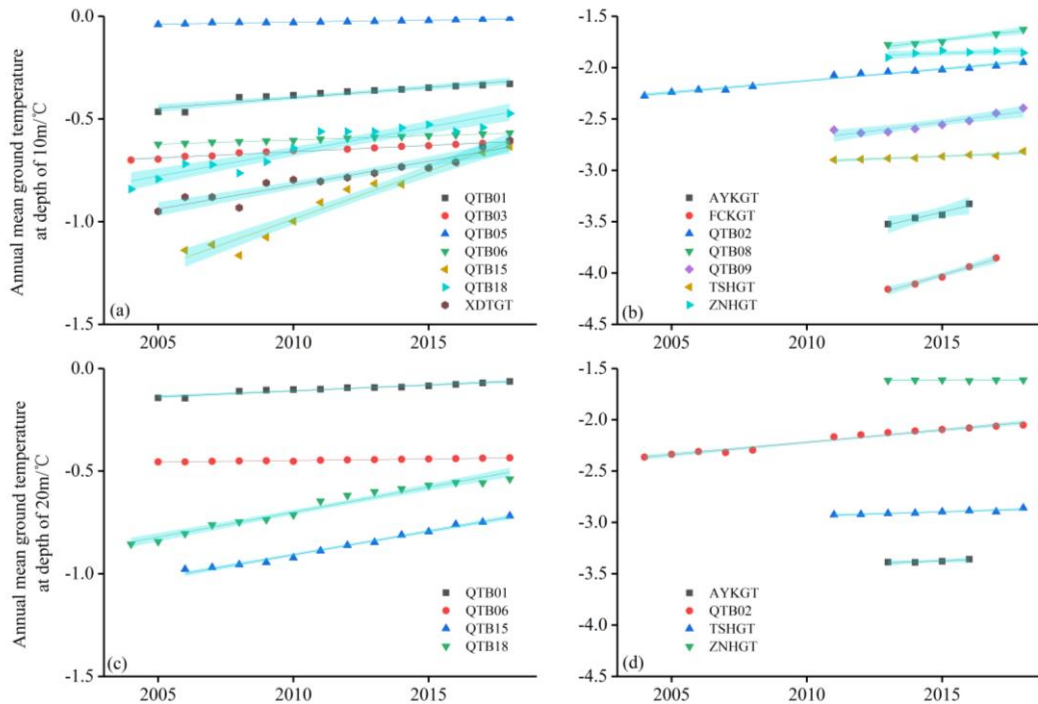
319

Figure 9. Variation in volumetric water content and soil water equivalent among different sites

320 3.3 Permafrost temperature

321 Fifteen borehole sites automatically collected GT at different depths; 14 are located in the
322 permafrost regions and only one is located in a structural talik region (QTB11). Annual mean GTs
323 at depths of 3 m and 6 m are given. The GT of these two horizons at most sites has obvious seasonal
324 variation and has remarkable inter-annual variation. Except for QTB11 locating in the seasonally
325 frozen ground region, the available mean annual GTs at 10 m and 20 m are shown in Fig. 10. For
326 the temperature of 10 m, the highest permafrost temperature appears at site QTB05 that locates in
327 the Qumar River along the Qinghai-Tibetan Road, the mean annual GT of which is very close to
328 0 °C. Meanwhile, the active layer thickness has approximately exceeded 9 m. The lowest
329 temperature appears at site FCKGT that locates in a high plain area in the south of Altun Mountain,
330 where the permafrost temperature reaches -4 °C due to extremely cold and dry climatic conditions.
331 The GT at all 15 boreholes showed significant linear increasing trends, and the permafrost has
332 warmed at different rates (Fig. 10). The warming rates at a depth of 10 m was ranged from
333 0.02 °C/decade (FCKGT) to 0.78 °C/decade (QTB05) but varied between 0 °C/decade and

334 0.24 °C/decade at a depth of 20 m. The annual mean temperature of 20 m at site ZNHGT has rarely
 335 changed during 2013-2018. At this depth, the most significant warming occurred at site QTB02,
 336 QTB18 and QTB15.



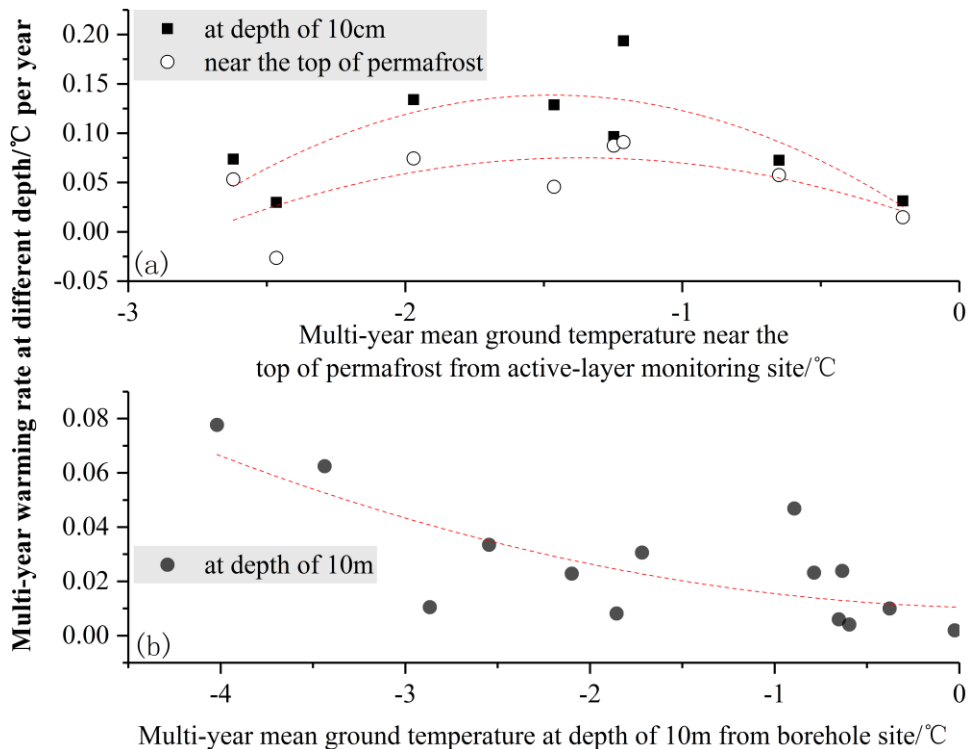
337
 338 **Figure 10.** Annual mean ground temperature as a function of time at a depth of (a, b) 10 m and (c, d) 20 m from
 339 borehole with continuous data series

340 The warming rate of permafrost seems to have a strong relationship with the temperature of
 341 permafrost itself. Fig. 11a shows that the change rate of GT at two shallow depths (10 cm and the
 342 depth near top of permafrost). They show an increasing trend first and then decreasing as the
 343 temperature near the bottom of the active layer rises. Both colder and warmer sites have a relatively
 344 lower variation rate of GT. The sites with GTs between -2 °C and -1 °C have the greatest ground
 345 warming rate. The warming of the active layer in permafrost regions may be mainly related to
 346 regional climate and local topography. Because most sites (QT1, QT3, QT8) with the largest
 347 warming rates are located on the high plain in the interior of the QTP, and they are geographically
 348 relatively close to each other. The two sites (CN1, CN6) with the lowest GT are located in the
 349 mountain areas (respectively belong to Fenghuo Mountain and Kunlun Mountain). At the same time,
 350 the other two sites (CN4, QT5) with the highest GT are located in the regions with the warmest
 351 climatic conditions, although the underlying surfaces are substantially different. Further study is

352 necessary because the current number of sites is far from enough.

353 However, the deep GT shows another pattern and lower temperature permafrost tend to have a
354 great warming rate (Fig. 11b). It is consistent with the previous research at the QTP, and the
355 correlation between permafrost temperatures and warming rates is more significant than the
356 previous. It indicates that the ice-water phase transition effect in the conversion from permafrost to
357 melting soil has significantly slowed GT increase.

358 We also analyzed another 69 sites, of which the GTs were recorded manually. The altitude of
359 these sites ranges from 4142 to 5247 m a.s.l. The drilling depth of the borehole reached 10 m at
360 most of the sites, and several reach 20 m. The observation interval is once every one year or two
361 years., the multi-year averages based on single observations are calculated to compare the thermal
362 regime of different sites. The multi-year mean GT of 10 m observed at different sites ranged from -
363 3.84 °C to 3.36 °C. There are 10 observation fields with a positive mean GT of 10 m and 59 fields
364 with negative values. The site with the highest GT is HT01, and the one with the lowest temperature
365 is STG. For all observation sites, the GT shows a slightly downward trend as the elevation increases.



366

367 **Figure 11.** The relationship between warming rate and multi-year mean ground temperature during observation

368

period from (a) active-layer monitoring site and (b) borehole site.

369 **4 Data availability**

370 All datasets in this paper have been released and can be free download from the National Tibetan
371 Plateau/Third Pole Environment Data Center ([https://data.tpdc.ac.cn/en/disallow/789e838e-16ac-](https://data.tpdc.ac.cn/en/disallow/789e838e-16ac-4539-bb7e-906217305a1d/)
372 [4539-bb7e-906217305a1d/](https://data.tpdc.ac.cn/en/disallow/789e838e-16ac-4539-bb7e-906217305a1d/),doi: 10.11888/Geocry.tpdc.271107), and more information about the
373 Permafrost Monitoring Network on the Qinghai-Tibet Plateau can be found at Cryosphere Research
374 Station on Qinghai-Xizang Plateau (<http://new.crs.ac.cn/>).

375 **5 Conclusions**

376 The observation data in permafrost regions on the QTP can provide basic data for studying
377 land-atmosphere interaction and climate change research. They could provide accurate inputs and
378 verifications for land surface models, reanalysis data and remote-sensing products, and climate
379 models. The results revealed that the annual mean air temperatures of all 6 sites are between -2.3 ~
380 -6 °C, and their seasonal variation characteristics are significant. Precipitation shows a significant
381 seasonal change trend, which is closely related to the monsoon period. The annual mean air
382 temperature of the XDT and TGL stations showed increasing trends, with rates of 0.66 and 0.40
383 °C/10a, respectively, and the GT has significant warming trend. The precipitations show an
384 insignificant week decrease trend. The active layer thickness has a slow increase trend with inter-
385 annual fluctuation, and their increasing amplitudes are very different amount different monitoring
386 sites. In addition, the high-quality comprehensive dataset with a focus on permafrost thermal state
387 on the QTP could provide accurate and effective forcing data and evaluation data for different
388 models. This valuable permafrost dataset is worth maintaining and promoting in the future due to
389 hard-won. It also provides a prototype of basic data collection and management for other permafrost
390 regions.

391

392 **Author contributions.** L Zhao generated and designed the observation network, participated
393 in the field installation of most observation sites, found supports for maintaining the observation
394 systems. DF Zou, GJ Hu, TH Wu, XD Wu, R Li, EJ Du, GY Liu, YP Qiao and X Yao participated
395 in the field works and maintained the observation sites. GJ Hu, R Li, EJ Du, GY Liu, X Yao and
396 DF Zou performed data processing, organization and analyses. GJ Hu, L Zhao, EJ Du, GY Liu, X
397 Yao and DF Zou wrote the paper, and all authors participated in the revision of the manuscript.

398 **Competing interests.** No conflict of interest.

399 **Acknowledgements.** We would like to thank all the scientists, engineers, and students who
400 participated in the field work and maintain this observation network and data acquisition.

401 **Financial support.** This work was financially supported by the National Natural Science
402 Foundation of China (41931180), the Second Tibetan Plateau Scientific Expedition and Research
403 (STEP) program, China (2019QZKK0201), and the National Natural Science Foundation of China
404 (42071094, 41701073).

405

406 **Reference:**

407 Bao, H., Koike, T., Yang, K., Wang, L., Shrestha, M., and Lawford, P.: Development of an enthalpy-
408 based frozen soil model and its validation in a cold region in China, *J. Geophys. Res.-Atmos.*, 121,
409 5259-5280, <https://doi.org/10.1002/2015jd024451>, 2016.

410 Chen, B., Luo, S., Lu, S., Zhang, Y., and Ma, D.: Effects of the soil freeze-thaw process on the regional
411 climate of the Qinghai-Tibet Plateau, *Climate Research*, 59, 243-257, <https://doi.org/10.3354/cr01217>,
412 2014.

413 Cheng, G., and Jin, H.: Groundwater in the permafrost regions on the Qinghai-Tibet Plateau and it
414 changes, *Hydrogeology & Engineering Geology*, 40, 1-11, 2013.

415 Cheng, G., Zhao, L., Li, R., Wu, X., Sheng, Y., Hu, G., Zou, D., Jin, H., Li, X., and Wu, Q.: Characteristic,
416 changes and impacts of permafrost on Qinghai-Tibet Plateau, *Chinese Science Bulletin*, 64, 2783-2795,
417 2019.

418 Cuo, L., Zhang, Y., Bohn, T. J., Zhao, L., Li, J., Liu, Q., and Zhou, B.: Frozen soil degradation and its
419 effects on surface hydrology in the northern Tibetan Plateau, *Journal of Geophysical Research:*
420 *Atmospheres*, 120, 8276-8298, <https://doi.org/10.1002/2015JD023193>, 2015.

421 Hu, G., Zhao, L., Wu, X., Li, R., Wu, T., Xie, C., Qiao, Y., Shi, J., Li, W., and Cheng, G.: New Fourier-
422 series-based analytical solution to the conduction-convection equation to calculate soil temperature,
423 determine soil thermal properties, or estimate water flux, *International Journal of Heat and Mass*
424 *Transfer*, 95, 815-823, <https://doi.org/10.1016/j.ijheatmasstransfer.2015.11.078>, 2016.

425 Hu, G., Zhao, L., Li, A. R., Wu, X., Wu, T., Zhu, X., Pang, Q., Liu, G. Y., Du, E., Zou, D., Hao, J., and
426 Li, W.: Simulation of land surface heat fluxes in permafrost regions on the Qinghai-Tibetan Plateau
427 using CMIP5 models, *Atmospheric Research*, 220, 155-168,
428 <https://doi.org/10.1016/j.atmosres.2019.01.006>, 2019a.

429 Hu, G., Zhao, L., Wu, X., Wu, T., Li, R., Xie, C., Xiao, Y., Pang, Q., Liu, G., Hao, J., Shi, J., and Qiao,
430 Y.: Variations in soil temperature from 1980 to 2015 in permafrost regions on the Qinghai-Tibetan
431 Plateau based on observed and reanalysis products, *Geoderma*, 337, 893-905,
432 <https://doi.org/10.1016/j.geoderma.2017.07.017>, 2019b.

433 Hu, G., Zhao, L., Zhu, X., Wu, X., Wu, T., Li, R., Xie, C., and Hao, J.: Review of algorithms and
434 parameterizations to determine unfrozen water content in frozen soil, *Geoderma*, 368, 114277,
435 <https://doi.org/10.1016/j.geoderma.2020.114277>, 2020.

436 Li, R., Zhao, L., Ding, Y., Wu, T., Xiao, Y., Du, E., Liu, G., and Qiao, Y.: Temporal and spatial variations
437 of the active layer along the Qinghai-Tibet Highway in a permafrost region, *Chinese Science Bulletin*,
438 57, 4609-4616, <https://doi.org/10.1007/s11434-012-5323-8>, 2012.

439 Li, X., and Koike, T.: Frozen soil parameterization in SiB2 and its validation with GAME-Tibet

440 observations, *Cold Regions Science and Technology*, 36, 165-182, <https://doi.org/10.1016/s0165->
441 232x(03)00009-0, 2003.

442 Liu, X., and Hou, P.: Relationship between the climatic warming over the Qinghai -Xizang Plateau and
443 its surrounding areas in recent 30 years and the elevation, *Plateau Meteorology*, 17, 245-245, 1998.

444 Ma, L., Zhang, T., Li, Q., Frauenfeld, O. W., and Qin, D.: Evaluation of ERA-40, NCEP-1, and NCEP-2
445 reanalysis air temperatures with ground-based measurements in China, *J. Geophys. Res.-Atmos.*, 113,
446 <https://doi.org/10.1029/2007jd009549>, 2008.

447 Ma, Y., Ma, W., Zhong, L., Hu, Z., Li, M., Zhu, Z., Han, C., Wang, B., and Liu, X.: Monitoring and
448 Modeling the Tibetan Plateau's climate system and its impact on East Asia, *Scientific Reports*, 7,
449 <https://doi.org/10.1038/srep44574>, 2017.

450 Ping, C., Jastrow, J., Jorgenson, M., Michaelson, G., and Shur, Y.: Permafrost soils and carbon cycling,
451 *Soil*, 1, 147-171, <https://doi.org/10.5194/soil-1-147-2015>, 2015.

452 Qiu, J.: The third pole, *Nature*, 454, 393-396, <https://doi.org/10.1038/454393a>, 2008.

453 Schuur, E., McGuire, A., Schädel, C., Grosse, G., Harden, J., Hayes, D., Hugelius, G., Koven, C., Kuhry,
454 P., and Lawrence, D.: Climate change and the permafrost carbon feedback, *Nature*, 520, 171-179,
455 <https://doi.org/10.1038/nature14338>, 2015.

456 Schuur, E. A. G., Abbott, B., and Permafrost Carbon, N.: High risk of permafrost thaw, *Nature*, 480, 32-
457 33, <https://doi.org/10.1038/480032a>, 2011.

458 Sharkhuu, A., Sharkhuu, N., Etzelmüller, B., Heggem, E. S. F., Nelson, F. E., Shiklomanov, N. I.,
459 Goulden, C. E., and Brown, J.: Permafrost monitoring in the Hovsgol mountain region, Mongolia,
460 *Journal of Geophysical Research Atmospheres*, 112, 195-225, <https://doi.org/10.1029/2006JF000543>,
461 2007.

462 Su, F., Duan, X., Chen, D., Hao, Z., and Cuo, L.: Evaluation of the Global Climate Models in the CMIP5
463 over the Tibetan Plateau, *Journal of Climate*, 26, 3187-3208, <https://doi.org/10.1175/JCLI-D-12->
464 00321.1, 2013.

465 Wang, G., Li, Y., Wu, Q., and Wang, Y.: Impacts of permafrost changes on alpine ecosystem in Qinghai-
466 Tibet Plateau, *Science in China Series D: Earth Sciences*, 49, 1156-1169, 2006a.

467 Wang, G., Li, Y., Wu, Q., and Wang, Y.: Impacts of permafrost changes on alpine ecosystem in Qinghai-
468 Tibet Plateau, *Science in China Series D-Earth Sciences*, 49, 1156-1169,
469 <https://doi.org/10.1007/s11430-006-1156-0>, 2006b.

470 Wang, L., Zhou, J., Qi, J., Sun, L., Yang, K., Tian, L., Lin, Y., Liu, W., Shrestha, M., Xue, Y., Koike, T.,
471 Ma, Y., Li, X., Chen, Y., Chen, D., Piao, S., and Lu, H.: Development of a land surface model with
472 coupled snow and frozen soil physics, *Water Resour. Res.*, 53, 5085-5103,
473 <https://doi.org/10.1002/2017wr020451>, 2017.

474 Wang, S. L., Jin, H. J., Li, S. X., and Zhao, L.: Permafrost degradation on the Qinghai-Tibet Plateau and
475 its environmental impacts, *Permafrost and Periglacial Processes*, 11, 43-53, 2000.

476 Wu, B., Yang, K., and Zhang, R.: Eurasian snow cover variability and its association with summer rainfall
477 in China, *Advances in Atmospheric Sciences*, 26, 31-44, 2009.

478 Wu, Q., Shen, Y., and Shi, B.: The relationship between frozen soil together with its water-heat process
479 and ecological environment in the Tibetan Plateau, *Journal of Glaciology and Geocryology*, 25, 250-
480 255, 2003.

481 Wu, X., Zhao, L., Chen, M., Fang, H., Yue, G., Chen, J., Pang, Q., Wang, Z., and Ding, Y.: Soil Organic
482 Carbon and Its Relationship to Vegetation Communities and Soil Properties in Permafrost Areas of the
483 Central Western Qinghai-Tibet Plateau, China, *Permafrost and Periglacial Processes*, 23, 162-169,

484 <https://doi.org/10.1002/ppp.1740>, 2012.

485 Yang, K., Wang, C., and Li, S.: Improved Simulation of Frozen-Thawing Process in Land Surface Model
486 (CLM4.5), *J. Geophys. Res.-Atmos.*, 123, 13238-13258, <https://doi.org/10.1029/2017jd028260>, 2018.

487 Yao, T., Piao, S., Shen, M., Gao, J., Yang, W., Zhang, G., Lei, Y., Gao, Y., Zhu, L., Xu, B., Yu, W., and
488 Li, S.: Chained Impacts on Modern Environment of Interaction between Westerlies and Indian
489 Monsoon on Tibetan Plateau, *Bulletin of the Chinese Academy of Sciences*, 32, 976-984, 2017.

490 Ye, D., and Gao, Y.: *The Meteorology of the Qinghai-Xizang (Tibet) Plateau*, Science Press: Beijing, 278
491 pp., 1979.

492 Zhang, Y., Carey, S. K., and Quinton, W. L.: Evaluation of the algorithms and parameterizations for
493 ground thawing and freezing simulation in permafrost regions, *J. Geophys. Res.-Atmos.*, 113,
494 <https://doi.org/10.1029/2007jd009343>, 2008.

495 Zhao, L., Ping, C.-L., Yang, D., Cheng, G., Ding, Y., and Liu, S.: Changes of climate and seasonally
496 frozen ground over the past 30 years in Qinghai–Xizang (Tibetan) Plateau, China, *Global and
497 Planetary Change*, 43, 19-31, <https://doi.org/10.1016/j.gloplacha.2004.02.003>, 2004.

498 Zhao, L., and Sheng, Y.: *Permafrost survey manual*, Science Press: Beijing, 13-14 pp., 2015.

499 Zhao, L., Wu, T., Xie, C., Li, R., Wu, X., Yao, J., Yue, G., and Xiao, Y.: Support Geoscience Research,
500 Environmental Management, and Engineering Construction with Investigation and Monitoring on
501 Permafrost in the Qinghai-Tibet Plateau, China, *Bulletin of the Chinese Academy of Sciences*, 32,
502 1159-1168, 2017.

503 Zhao, L., Wu, X., Wang, Z., Sheng, Y., Fang, H., Zhao, Y., Hu, G., Li, W., Pang, Q., Shi, J., Mo, B., Wang,
504 Q., Ruan, X., Li, X., and Ding, Y.: Soil organic carbon and total nitrogen pools in permafrost zones of
505 the Qinghai-Tibetan Plateau, *Scientific Reports*, 8, <https://doi.org/10.1038/s41598-018-22024-2>, 2018.

506 Zhao, L., Hu, G., Zou, D., Wu, X., Ma, L., Sun, Z., Yuan, L., Zhou, H., and Liu, S.: Permafrost Changes
507 and Its Effects on Hydrological Processes on Qinghai-Tibet Plateau, *Bulletin of the Chinese Academy
508 of Sciences*, 34, 1233-1246, 2019.

509 Zhao, L., Zou, D. F., Hu, G., Du, E., Pang, Q., Xiao, Y., Li, R., Sheng, Y., Wu, X., Sun, Z., Wang, L.,
510 Wang, C., Ma, L., Zhou, H., and Liu, S.: Changing climate and the permafrost environment on the
511 Qinghai–Tibet(Xizang) Plateau, *Permafrost and Periglac Process*, 1-10,
512 <https://doi.org/10.1002/ppp.2056>, 2020.

513 Zou, D., Zhao, L., Sheng, Y., Chen, J., Hu, G., Wu, T., Wu, J., Xie, C., Wu, X., Pang, Q., Wang, W., Du,
514 E., Li, W., Liu, G., Li, J., Qin, Y., Qiao, Y., Wang, Z., Shi, J., and Cheng, G.: A new map of permafrost
515 distribution on the Tibetan Plateau, *Cryosphere*, 11, 2527-2542, [https://doi.org/10.5194/tc-11-2527-](https://doi.org/10.5194/tc-11-2527-2017)
516 2017, 2017.